

# BarraCUDA: Bringing Electromagnetic Side Channel Into Play to Steal the Weights of Neural Networks from NVIDIA GPUs

Péter Horváth\*, Łukasz Chmielewski†, Leo Weissbart\*, Lejla Batina\*, Yuval Yarom‡

\*Radboud University

†Masaryk University

‡Ruhr University Bochum

**Abstract**—Over the last decade, applications of neural networks have spread to cover all aspects of life. A large number of companies base their businesses on building products that use neural networks for tasks such as face recognition, machine translation, and autonomous cars. They are being used in safety and security-critical applications like high definition maps and medical wristbands, or in globally used products like Google Translate and ChatGPT. Much of the intellectual property underpinning these products is encoded in the exact configuration of the neural networks. Consequently, protecting these is of utmost priority to businesses. At the same time, many of these products need to operate under a strong threat model, in which the adversary has unfettered physical control of the product.

Past work has demonstrated that with physical access, attackers can reverse engineer neural networks that run on scalar microcontrollers, like ARM Cortex M3. However, for performance reasons, neural networks are often implemented on highly-parallel general purpose graphics processing units (GPGPUs), and so far, attacks on these have only recovered course-grained information on the structure of the neural network, but failed to retrieve the detailed weights and biases.

In this work, we present BarraCUDA, a novel attack on GPGPUs that can completely extract the parameters of neural networks. BarraCUDA uses correlation electromagnetic analysis to recover the weights and biases in the convolutional layers of neural networks. We use BarraCUDA to attack the popular NVIDIA Jetson Nano device, demonstrating successful reverse engineering of neural networks in a highly parallel and noisy environment.

## 1. Introduction

The field of machine learning has seen an explosive increase in interest and use over the last decade. In particular, deep learning has proven to be a versatile technique that provides state-of-the-art performance for many real-world application. The use of deep learning proved useful for a broad range of domains including playing chess [50], object detection [35], image classification [17, 23, 29, 34, 51], audio processing [43], forecasting [31, 45, 47, 48] and

natural language processing [40]. Thus, applications of deep learning are changing many areas of our lives and have become indispensable to our everyday life.

Deep learning typically utilizes artificial neural networks, consisting of multiple layers of (simulated) neurons. In a nutshell, a neuron takes a number of inputs and computes a non-linear function of the weighted sum of the inputs. A common example of such a function is a rectified linear unit (ReLU), which basically returns its input if it is positive and zero otherwise. When designing a deep learning solution for a problem, the designer first chooses the network architecture, which specifies the layers of neurons, including their sizes and types, as well as how the neurons are connected, i.e. which neurons outputs are connected to which inputs. The designer then trains the network, selecting the weights used for each weighted sum as well as bias values that are added to the sums before the computation of the non-linear function.

Training a network for any non-trivial example is a resource intensive process. There is a need to curate a specialized dataset of correctly labeled samples that can be used for the training, and the training process often requires days and even weeks of computation on specialized high-performance hardware, such as large quantities of graphical processing units (GPUs). Moreover, the design of the right network architecture for a given purpose requires specialized expertise. Consequently, the design and parameters of trained models are in many cases considered as trade secrets, which vendors try to protect against undesired disclosure.

Side-channel attacks, which exploit information leakage via unintended effects of performing computation, are a major threat to the confidentiality of deep learning designs. Such attacks against neural network implementations on CPUs have been demonstrated using both power analysis [13] and microarchitectural attacks [54], among others. However, to achieve a better performance neural networks are often implemented on GPUs. So far, attacks on such implementations only recover the network architecture, but not the parameters [16, 37]. Moreover, these attacks only target open-source neural networks, implemented using PyTorch [41] and TensorFlow [12], while we target the commonly used NVIDIA closed-source TensorRT frame-

work [10].

Therefore, this work focuses on the following research questions:

*Are implementations of neural networks on GPU vulnerable to parameter extraction using side-channel analysis?*

## Our Contribution

In this work we answer the question in the affirmative. We analyze NVIDIA’s closed-source neural network framework TensorRT [10] executing on an industrial-strength Jetson Nano device [9]. While TensorRT is a closed-source framework, the produced CUDA binaries can be disassembled.

We demonstrate a side-channel attack that monitors the electromagnetic (EM) emanations emitted from the device. The attack allows full extraction of the parameters of the neural network running on the device, overcoming the measurement noise and the uncertainty inherent in closed platforms.

The attack uses correlation electromagnetic analysis (CEMA) to recover the weights and biases of neural networks. For the attack, we collect and process 15 million traces over a period of 10 days. We then show how to analyze the traces to recover weights and biases used in the target network.

The results of attack demonstrate that GPU implementations of deep learning are not protected against side-channel attacks, even when the source code is not available.

**Disclosure.** We notified NVIDIA of the found vulnerabilities on September 22nd, 2023. We shortly received a response on 24/09/2023 that they are looking into our findings and as a result of mutual agreement the findings would be not released until December 13rd, 2023. On November 22nd, 2023 NVIDIA notified us that they reviewed our disclosure and classified the vulnerabilities as a low severity issue while also recommending the users to follow guidelines to prevent physical access to secure systems to avoid information leakage.

**Organization.** The rest of this paper is organized as follows: After providing the necessary background on side-channel attacks and GPU architecture (Section 2), we describe our weight extraction attack. in Section 3. Finally, Section 4 covers the limitations, possible extensions, countermeasures, and related work.

## 2. Background

Here we introduce the concepts of side channels and related techniques that were used for the attacks and provide background on NVIDIA’S CUDA programming model and GPU architecture.

### 2.1. Side-Channel Analysis

Side-Channel Analysis (SCA) exploits the physical leakages of electronic devices to extract secret information [27,

28]. Leakage can occur through various channels, including power consumption, electromagnetic, timing, optical or sound, and various types of secret information can leak. In academic settings, side-channel attacks were first introduced in the 90’s targeting constrained cryptographic devices [27, 28] and pose ever since a constant threat to the security of various embedded systems. In this work, we exploit the EM side channel.

**2.1.1. Electromagnetic emanation.** The electromagnetic (EM) emanations from a computing device correlate with the code and the data that the device processes. This correlation has been used to break cryptographic implementations [30, 44], reverse engineer neural networks [13, 16] and eavesdrop on display units [20, 24, 36].

In Simple EM Analysis (SEMA), the attacker samples the emitted signal during the execution of the target program, creating a *trace* of measurements. The attacker then analyzes the trace to identify components that correspond to the secret information.

In Correlation EM Analysis (CEMA), the attacker builds a model of the leakage based on the data the program processes. The attacker then executes the program multiple times with different inputs, and looks for correlation between the predicted leakage based on the model and the observed leakage at some points of interest (POIs) in the collected traces. Two common models are the Hamming weight (HW) model, which predicts that the leakage is linear with the number of set bits in the data (i.e. its Hamming weight), and the Hamming distance (HD) model, which predicts that the leakage is linear with the number of bits that need to be changed between consecutive data values.

**2.1.2. Leakage evaluation.** Multiple methods have been proposed to evaluate the leakage of embedded devices, such as intermediate correlation, Test Vector Leakage Assessment (TVLA) [49] and  $\chi^2$ -test [39]. In this paper, we use intermediate correlation and TVLA to place our EM probe at a location that leaks the most information and detect where each intermediate value leaks in the collected measurements in the parameter extraction attack presented in Section 3.

### 2.2. CUDA programming model

To leverage the parallelism offered by GPUs, NVIDIA exposes the CUDA programming model [5] to developers. In this model, multiple abstraction levels exist and each level has different implications with respect to the GPU hardware. The lowest level of abstraction is the `thread`, which executes a CUDA function defined by the developer. The number of threads executing the CUDA function in parallel is specified at the time of invoking the function.<sup>1</sup> Subsequently, multiple threads can be grouped together into a single `block` of threads. Threads in a block have a per block on-chip shared memory region where they can

1. Functions in CUDA are also called *kernels*. We use the term function to avoid confusion with kernels in CNNs.

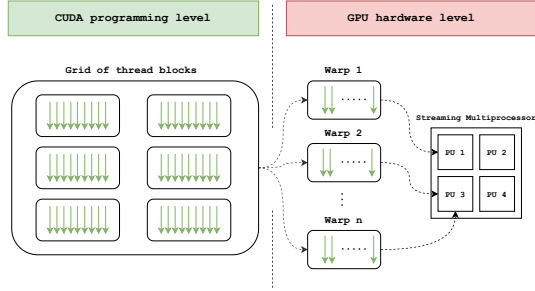


Figure 1: CUDA programming interface and GPU hardware implementation.

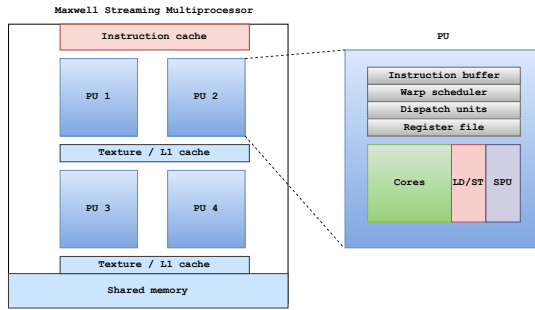


Figure 2: GPU Streaming Multiprocessor architecture.

exchange data with other threads in the block. Blocks of threads form a grid of thread blocks. Each block in a grid executes independently from the other blocks, but all blocks in the grid share the same off-chip global memory region.

### 2.3. GPU Streaming Multiprocessor

When a CUDA function is invoked, the parallel threads execute on the Streaming Multiprocessor (SM) of the GPU. A GPU can consist of one or more SMs to further improve parallelism. Our target, the Jetson Nano, features a Tegra X1 System-On-Chip that consists of one SM of the Maxwell architecture [11] and CUDA Compute Capability 5.3 [1] from NVIDIA. As illustrated in Figure 1, when blocks of threads are scheduled onto a particular SM, the threads in the blocks are divided into groups of 32 threads, also called warps. Warp is the lowest level of execution unit and is of great concern for SCA. Every warp is assigned to a particular Processing Unit (PU) where every PU has dedicated resources to schedule and execute warps in the SM. Figure 2 shows the building blocks of the Maxwell SM and the PUs in the SM.<sup>2</sup> The warp scheduler in a PU is responsible for scheduling and issuing instructions for warps that are ready. Every PU has a set of 32 CUDA cores for arithmetic instructions as well as load/store units (LD/ST) and special function units (SPU) for memory operations and transcendental functions, respectively. In addition, a pair of PUs share a texture/L1 cache but all PUs have access to

2. Graphics related components, such as the PolyMorph engine, are omitted in our figure as these are not relevant for our target application.

the same shared memory on the chip. More importantly for side-channel attacks, each PU also has a dedicated register file. Since the details of assigning individual warps to PUs are not publicly disclosed information, multiple register files could mean that a CPA/CEMA attack is significantly hindered. If a particular warp, one that calculates our targeted intermediate variable, is assigned to different PUs in subsequent executions, then our targeted intermediate variable is saved into multiple, different register files which potentially results in different power/EM signatures. Therefore, mounting side-channel attacks that rely on the HD leakage model might become difficult on the GPU, but we present a successful attack using the HW as well as the HD leakage model.

## 3. Weight and bias extraction attack

In this section, we detail our attack which recovers the weights and biases of a CNN with 2 convolutional layers, each containing one kernel. First, we describe the threat model and explore the NN implementations from NVIDIA on the assembly level. Second, we describe our experiment setup and the process of establishing points of interest (PoI) where the implementations leak information. Lastly, we apply CEMA on intermediate values in the convolution operation to extract the weights and bias of each layer. To the best of our knowledge, this is the first time that the weights and biases of NNs are extracted from implementations running on an NVIDIA GPU. In addition, the experiments are carried out using half-precision calculations in the convolutional layers.

### 3.1. Threat model

In this scenario, we consider an adversary who has access to the target device, can observe random inputs fed to the device, and knows the architecture of the NN that runs on the device. In addition, we also assume that the adversary can collect electromagnetic side-channel measurements. We assume that the architecture of the target NN is already extracted as the architecture of a NN needs to be known for the NN parameters to be extracted using CEMA.

### 3.2. Exploring TensorRT implementations

The approach of NVIDIA’s TensorRT framework is “one size fits many”, that is, one implementation can be used for layers with different kernel sizes, input sizes, batch sizes etc. TensorRT provides information [8] about the optimized model and this information includes the names of the CUDA function implementations that are used for the model as well as a hexadecimal undocumented value called *Tacticvalue*.<sup>3</sup> Using this information, it is possible to extract the assembly device code that is executed by each thread on the GPU. One

3. While there is no documentation about *Tacticvalue*, it might impact the implementation’s execution since it might be used in predicated instructions.

can use `cuobjdump` [4] from the CUDA toolkit to extract all the GPU assembly code that can be found in the different CUDA shared library files (CuBLAS, CuDNN, TensorRT). Eventually, we found the CUDA function corresponding to the implementation of a convolutional layer with ReLU activation in the `libnvinfer.so` file by the name that can be retrieved using the TensorRT API.

In our parameter extraction attack, we reverse engineer the weights of a NN with two convolutional layers each with a kernel containing 5 weights. In the shared library files, 4 implementations can be found for a convolutional layer with half-precision calculations and ReLU activation, named:

`maxwell_fp16x2_hcudnn_fp16x2_128x_k_relu_t_nn_v1`,

where

$$k \in \{32, 64, 128\},$$

$$t \in \{\text{small, medium, large, interior}\}.$$

Based on repeated testing, the *small*, *medium* and *interior* implementations can all be an implementation that the TensorRT API chooses for each convolutional layer in our 2-layer model configuration. This is possible if the timing differences are small in the implementations. Thus, it could be that the same implementation is used for both layers or a combination of two.

Furthermore, based on testing and using the information provided by the API [8], these are also the implementations that are chosen by the API for the large-scale neural networks such as MobileNet [25].

The names of implementations also include *fp16x2* which refers to the *half2* [6] data type in CUDA. When *half2* is used, a register is packed with 2 half-precision floating point values and the GPU can execute a floating point instruction on each half in parallel, doubling the throughput of the GPU, as opposed to using single-precision floating point values. This also means additional noise for SCA in addition to the parallel threads executing in the GPU.

### 3.3. Convolutional layer structure

Although there are 4 possible implementations for a convolutional layer with ReLU activation, these implementations are very similar in their structure and they consist of the following blocks:

1. block of initialization instructions,
2. block of convolution operations, and
3. block of bias addition and ReLU calculation.

**1. Init block.** The first main block consists of instructions to set up the CUDA function. In this block, 64 accumulator registers are initialized which are later used to calculate the sum of multiplications in the convolution operation.

**2. Convolutional block.** The second block is where the convolution operations are carried out. This block consists of vectorized load and HFMA2 instructions. In addition, it contains predicated load instructions from global memory. Since registers are packed with two 16-bit floating point



Figure 3: Location of the Langer EM probe. The probe tip is located between two capacitors.

values, it is also crucial to know exactly how the input data is loaded into the registers. If this information is available, it sheds light on how the convolution operation is carried out in the implementations. According to the API, the input is reformatted so that it is laid out in “*Two wide channel vectorized row major FP16 format*”. This means that each register holding inputs is loaded with two half-precision floating point inputs from two different input channels. Therefore, this also suggests that each register holds weights from different channels in a kernel. In the case of our one dimensional convolution, we set the number of input channels to 1, as it is common for one-dimensional convolutional use cases. In other cases, such as RGB image inputs, the number of input channels would be 3 so each register would hold input values from two different input channels. With multiple input channels processed in parallel, our CEMA attack would then not require more time to get all the weights because the channels in the kernels are independent from each other. Additionally, the code in the second block indicates that each accumulator register is used in 8 HFMA2 instruction in this block, unless a predicated jump instruction is executed at the end of the code block which jumps back to the start of this block. This suggests that the execution of the jump instruction likely depends on the kernel size in the layer.

**3. ReLU block.** The third block, repeated four times, first calculates the sum of the lower and higher half of each register. This suggests that the channel combinations of the convolutional operation, after the sum of multiplications, are executed in these blocks. Then, *half2* floating point additions and HSET instructions are executed in the block suggesting the calculation of the bias addition and the ReLU output.

Overall, the four implementations are very similar. For our particular two-layer model configuration, more than 50% of the times the chosen implementation by the API is the *relu\_small* implementation for both layers, so we choose to carry out the parameter extraction attack with this implementation. However, we also analyzed the *relu\_medium* and *relu\_interior* implementations in our leakage detection process in Section 3.6.

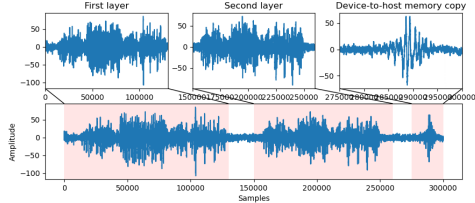


Figure 4: Raw trace of the whole operation on the GPU. The 2 layers are clearly separated in the traces. Additionally, the CUDA device-to-host memory copy is also clearly visible in the end of the trace.

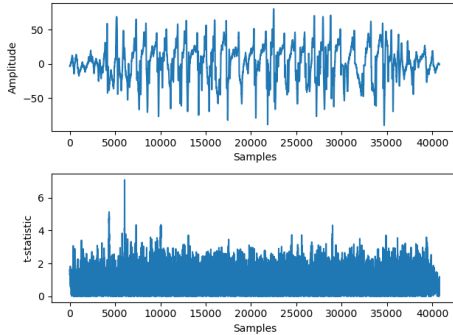


Figure 5: Result of TVLA for the multiplication with the first weight in the kernel in convolutional block. The top figure depicts an elastically aligned trace while the bottom figure shows the corresponding absolute t-test statistics at each time sample. There are multiple leaking spots with  $|t| > 4.5$  but the overall leakage is not high.

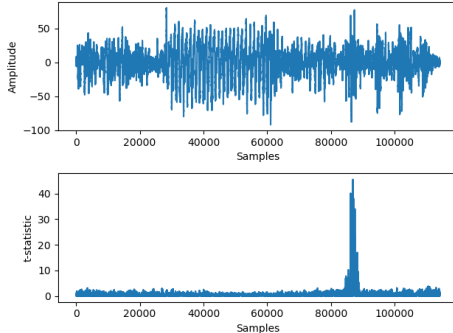


Figure 6: Result of fixed vs random bias TVLA. The top figure depicts an example trace while the bottom figure shows the corresponding absolute t-test statistics at each time sample. There is clear leakage scattered across multiple clock cycles with  $|t| >> 4.5$ .

### 3.4. Experiment setup

In our setup, the Jetson Nano’s GPU cores operate at the highest possible clock frequency at 921MHz. In order to collect electromagnetic traces, we use the Lecroy 8404M-MS oscilloscope at a sampling rate of 10GS/s with the

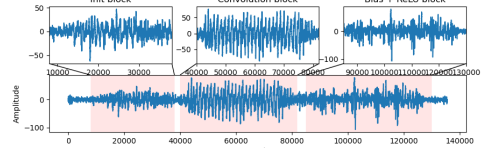


Figure 7: Segmented raw trace of first layer. The first highlighted block contains the initialization instructions. The second highlighted block is where the convolution operation is carried out. The third highlighted block corresponds to the bias addition and ReLU activation calculation.

Langer MFA-R 0.275 near-field probe [7]. Each trace contains measurements of the electromagnetic emanations of the GPU when the target neural network executes inference on random inputs. By scanning the Tegra SoC and the nearby capacitors with the EM probe, we found multiple interesting locations that leak information about the parameters of neural network. Eventually, we observed the best signal between two capacitors, as shown in Figure 3. In terms of leakage magnitude using TVLA, locations above the chip and between the capacitors are very similar. However, the emitted signal between the capacitors provides less noisier traces which makes trace acquisition and alignment easier. To trigger the oscilloscope to collect measurements when the inference of the NN starts, we use the rising edge of inference signal as trigger.

### 3.5. Trace preprocessing

Figure 4 shows an example trace of the inference operation of a CNN with two layers. The two layers are clearly separated and display similar patterns. However, the first layer takes considerably more time to execute. Since the input sizes of the layers are 500 and 496, respectively, this difference alone might not explain the observed difference in execution times. However, the GPU has various caches which might explain this behaviour. More importantly, we observed that different patterns can repeat in the second layer from trace to trace. Whereas the patterns are very similar in the first layer for all collected traces, the same does not hold for the second layer. For the second layer, only about 40% of the collected traces display completely similar patterns. We tested this behaviour with the other implementations as well and this issue only comes up when the same implementation is used for each layer. For example, the combination of the *relu\_small* and *relu\_interior* implementations for the first and second layers, respectively, result in uniform patterns for both layers. In contrast, if the *relu\_small* implementation is used for both layers, then it results in non-uniform patterns for the second layer. We also tested this behaviour with networks with more than two convolutional layers, and as soon as the same implementation is used in two different layers the non-uniform behaviour is encountered. Regardless, as mentioned in Section 3.2, we carry out the parameter extraction with the *relu\_small* as the used implementation for each layers.

Since accurate alignment with static alignment [38]<sup>4</sup> is not possible using all of the traces for the second layer, 60% of the collected traces are not used in the CEMA attack for the second layer.

In addition, despite collecting measurements with minimum misalignment, the traces are hard to fully synchronize as they contain lot of jitter. To combat this problem, we use elastic alignment [52] in the leakage detection process. Elastic alignment allows us to align the traces at every time point, however, it is also a technique that requires tuning the correct parameters and it is computationally expensive to do so. Therefore, it is used only to align traces to detect leaking points but the CEMA attack is carried out on the raw traces which are aligned using static alignment.

### 3.6. Leakage detection

Detecting where intermediate values might leak is a necessary step before applying CEMA. In order to do so, we apply random vs fixed TVLA [21] and intermediate correlation to detect PoIs in both layers. We also used leakage detection process to decide the best location for the probe in our setup. Furthermore, we performed the leakage detection on the *relu\_small*, *relu\_medium* and *relu\_interior* implementations and the analysis presented in this section applies to all three.

The TensorRT framework supports refitting networks on-the-fly with different weights but a new CUDA context [2] has to be created every time the network is refitted with new weights as per the documentation. Normally, an application is not required to create a new CUDA context for every inference operation, but it is required for TVLA as we refit the weights or the bias for every inference operation.

To the detect PoIs, we applied TVLA 5 times, which is equal to the kernel size, each time with one weight in the convolutional kernel being fixed vs random and the rest of the weights 0. The corresponding first input, with which the weight is multiplied, is fixed and non-zero while the rest of the inputs are set to 0. This setup allows us to detect leakages corresponding to the partial sums in the convolutional operation. In this case, the unexploitable false positives can be loading of the weights. The presented approach is more desired, i.e. leads to less false positives, then applying TVLA with random vs fixed inputs as the same input is loaded at different times, potentially leading to more false positives.

In addition, to detect leakage corresponding to the bias, we apply fixed vs. random bias TVLA. Similarly to the random vs. fixed weight TVLA, the false positives in this test can be the loading of the bias. To help filtering these false positives, we also apply correlation to intermediate values. However, we also observed several ghost peaks [14, 15] with the correlation method which cannot be exploited in the CEMA attack.

4. Static align employs a standard pattern-based approach: we select a part of a trace as a reference, and compute correlation for each offset within a chosen range for each of the traces. We then shift each trace by the respective offset that maximizes the correlation.

Figure 5 shows the results of TVLA for the first weight in the kernel in the first layer with 45k traces. We repeat this process for the rest of the weights and the results clearly show that leakages of the convolution operation are in the second highlighted part of Figure 7. Figure 6 shows the results of TVLA for the bias of the kernel in the first layer with 37k traces. There is a much clearer leakage present for the bias than for the weights in the convolution operation.

After establishing the PoIs with the help of elastic alignment, we use static alignment on the raw traces at these points as static alignment produced higher individual TVLA peaks as well as correlation for the attack.

After the TVLA and correlations tests, it is possible to segment the raw traces according the instruction blocks mentioned in Section 3.2. Figure 7 shows a raw trace where the first highlighted section corresponds to the initialization block. The second highlighted block corresponds to the sum of multiplications in the convolution operation. The third highlighted segment corresponds to the calculation of the bias addition and ReLU output, repeated 4 times for different sets of registers. Note, that these instruction blocks are also separated by synchronization instructions which are also visible in the trace as the amplitude of the EM signal drops close to 0 between the blocks. The same segmentation applies for the second layer.

### 3.7. Weight and bias extraction

If an adversary is able to recover a neural network's architecture as well as the parameters of a network, then the adversary completely recovered the model. In this attack, we show how to extract the weights and the biases of a CNN with 2 layers using CEMA. Observe that this attack is general and can be extended to arbitrary number of convolutional layers with arbitrary dimensions: since the implementations in Section 3.2 are parallelized on a kernel and channel level, CEMA also can be parallelized to recover all the weights in a layer if an adversary has multiple machines available.

The input and batch size of our CNN are set to 500 and 1, respectively, while the weights and biases are initialized randomly. With an input size of 500 and stride of 1, the number of convolutions executed by a layer is *input\_size - kernel\_size + 1*. Consequently, the first and second layers execute 496 and 492 convolutions, respectively. This means there are lots of convolutional intermediates to target in each layer to recover the weights and bias of a kernel. However, our attack only requires knowing just a fraction of the inputs, and the size of this fraction is equivalent to the kernel size. Therefore, we only use the first 5 inputs to each layer to recover the weights and biases in the layers.<sup>5</sup>

The layers in our example consist of one kernel each containing 5 unknown weights and 1 unknown bias. The convolutional layers are followed by ReLU activation. Altogether, 12 unknowns have to be recovered from both layers.

5. However, in order to calculate the first 5 inputs to the second layer, the first 9 inputs to the first layer has to be known.

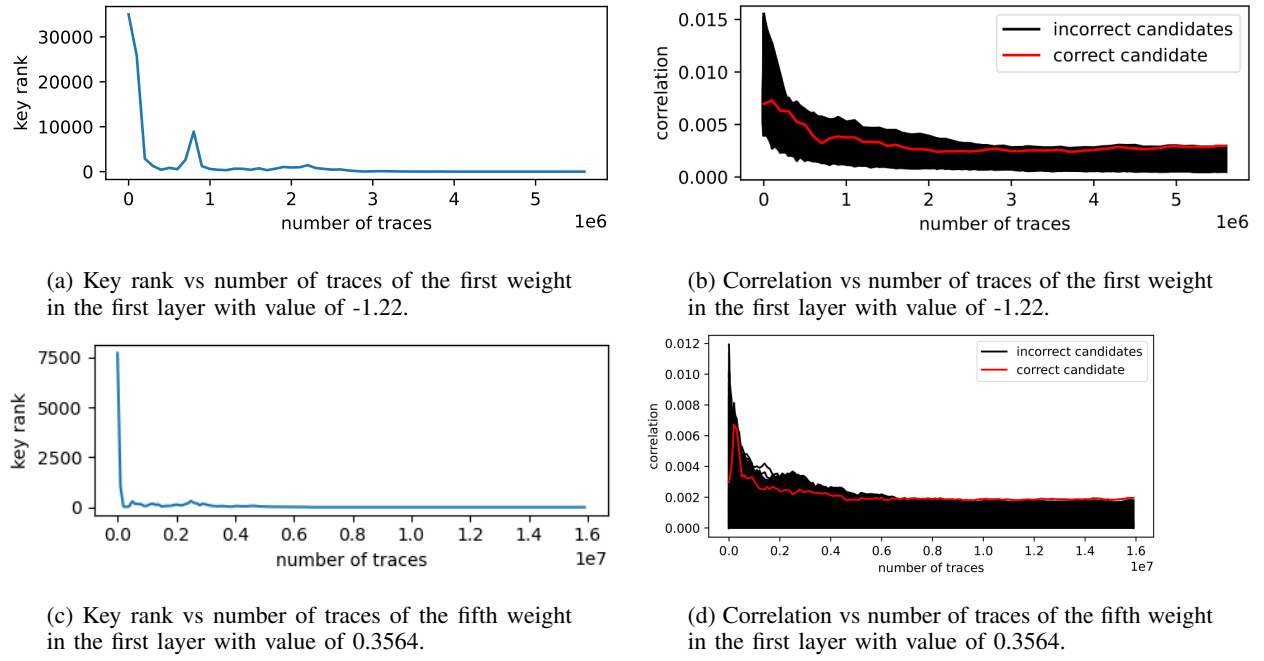


Figure 8: Key ranks and correlations of the first and fifth weights in the first layer.

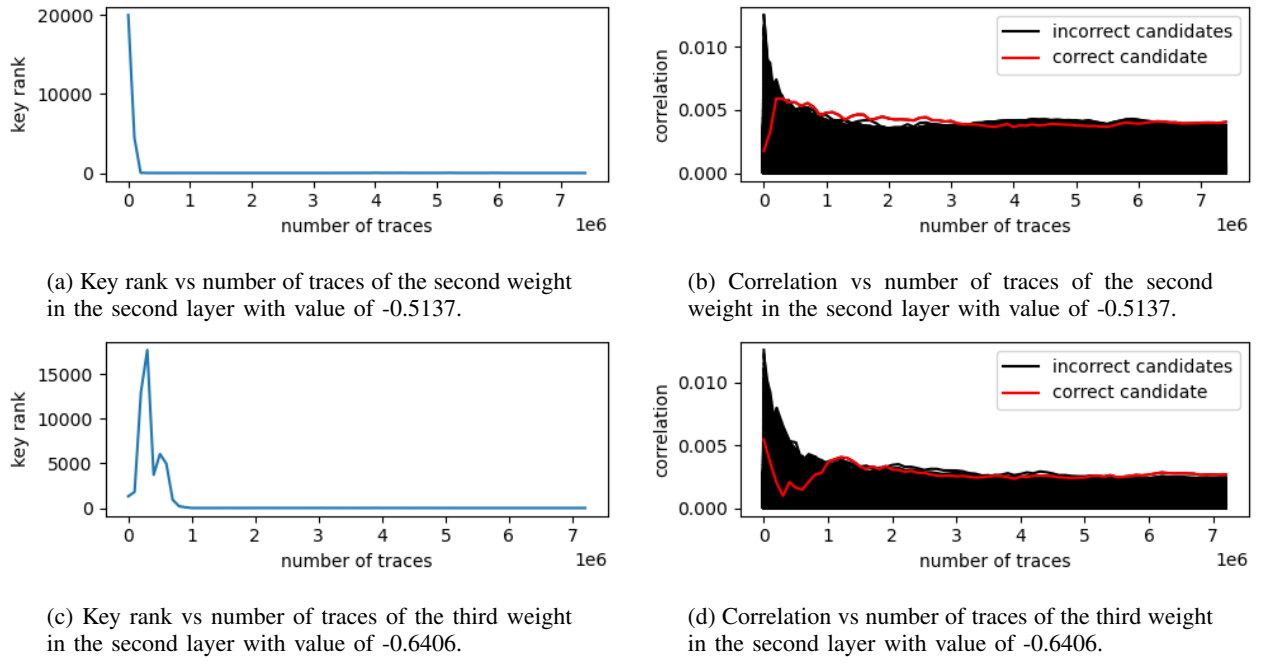


Figure 9: Key rank and correlation for the third and fourth weights in the kernel in the second layer.

Formally, each layer computes

$$\text{ReLU}(W * M + b) = \text{ReLU}\left(\sum_{i=1}^5 w_i \cdot m_i + b\right),$$

for a piece of input where  $W$  and  $M$  are vectors containing the kernel weights and layer inputs, respectively, and  $b$  is the bias that is added after the sum of multiplications. In this case, there are multiple intermediate values that depend on the secret weights. First, every weight  $w_i$  is multiplied by an input  $m_i$  so the results of the individual multiplications can be targeted. Second, the results of multiplications are summed. Afterward, the bias  $b$  is added to the accumulated results. Lastly, the ReLU activation is applied after the bias addition. All of these intermediate values depend on the unknown weights or the unknown bias. In the attack, we have to recover of the parameters of the layers sequentially, i.e. we have to recover the weights and bias in the first layer to be able to attack the second layer.

**3.7.1. Weight extraction.** In this experiment, we target the intermediate results of the convolution between the weights and the inputs, as we could observe results with this leakage. We present results with two different leakage models as using the HW leakage model on the partial sum intermediates and the HD between two subsequent intermediate allows us to extract the weights.

Following Batina et al. [13], we restrict the search space of the weights to the interval  $[-5, 5]$ . With 16-bit floats, there are 35 330 possible candidates in this range. We use the HW leakage model on our chosen intermediate value, the partial sums, to map hypothetical EM consumption values to real measurements  $T$  and calculate the Pearson’s correlation per sample point between them:

$$\rho(HW\left(\sum_{j=1}^i w_j \cdot m_j\right), T) \quad i = 1..5.$$

We calculate the correlation with each weight candidate, selecting the candidate that shows the highest correlation.

Figure 8 shows the key rankings and correlations of the correct weight value vs the number of traces in the first layer for the first and fifth weights, respectively. As shown in Figure 8a, at around the 3,2 million mark, the candidate that ranks first is  $-1.212$  for the first weight, so it is already a value that is close to the correct candidate. At this mark, the correct candidate ranks 106th. Overall, the key rank decreases quickly but in order to get the first rank for the correct candidate, more than 5 million traces are required. This might suggest that the exponent of the intermediate values leak mostly but not the mantissa, and it requires significantly more traces to get the correct candidate. We leave analyzing this phenomenon for future work.

Figure 8b shows the correlation of the correct weight candidate and the incorrect weight candidates vs the number of traces for the first weight. As expected, it shows a similar trend to the key rank figure, as the correlation of the correct candidate gets close to the top at the 3 million traces mark.

However, the correlation of the correct weight candidate only reaches the maximum after 5 million traces with respect to the incorrect candidates. Figure 8c shows the ranking of the correct weight value vs the number of traces in the first layer for the fifth weight. Similarly to the first weight, the key rank drops quickly, but it takes a lot more traces to for the key rank to converge zero. Similarly, Figure 8d shows the correlation of the weight candidates vs the number of traces for the fifth weight in the first layer. The correct weight candidates already approaches key rank 0 at 8 million mark while needing more traces to fully converge. Every weight in the kernel leaks similarly and targeting the Hamming weight of partial sums can recover the correct weight candidate for all the weight in the kernel. After recovering the weights and bias of the kernel in the first layer, we can calculate the inputs to the second layer to recover the weights and the bias of the kernel in second kernel. Figure 9 shows the key ranking and correlations of the correct weight value vs the number of traces in the second layer for the second and third weights, respectively. Similarly to the weights in the first layer, the key ranks for both weights drop quickly, but reaching a key rank of 0 requires 800 000 and 1.2 million traces for the second and third weights, respectively.

**3.7.2. Bias extraction.** There are two operations in the layer that are dependent on the bias value. The first operation is the calculation of the sum of convolution and the bias  $W * M + b$ . The second one is the ReLU output,  $\text{ReLU}(W * M + b)$ . We observed leakage with the Hamming weight of the sum of convolution and the bias, as well as with the output of the ReLU activation. Formally,  $HW(W * M + b)$  and  $HW(\text{ReLU}(W * M + b))$  both show correlation with the EM measurements. Therefore, we calculate the Pearson correlation for every bias candidate with these leakage models to the real measurements.

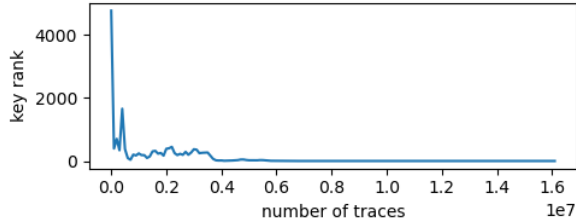
Figure 10 shows the key ranking and correlation of the CEMA attack on the bias in the first layer with the  $\text{ReLU}(W * M + b)$  intermediates. The key rank drops rapidly, but the convergence to key rank 0 takes more than 10 million traces. Similarly, Figure 10 shows the key rankings and correlation of the CEMA attack on the bias in the second layer with the  $W * M + b$  intermediate. The key rank also drops quickly for the bias in the second layer, but the convergence to key rank 0 takes more than 10 million traces. In general, the biases seem to require more traces to converge to key rank 0 than the weights.

## 4. Discussion

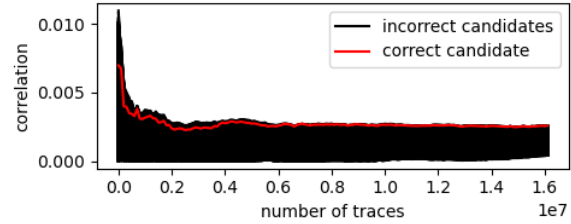
### 4.1. Limitations

**4.1.1. Parameter extraction.** In this work, we demonstrated the parameter extraction of a NN with two convolutional layers. However, there are multiple aspects that could impact the CEMA attack:

**Kernel size.** The kernel size does not impact the CEMA attack in terms of number of traces needed, but it would

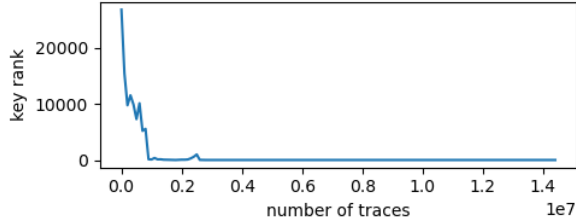


(a) Key rank vs number of traces of the bias in the first layer with the ReLU intermediate.

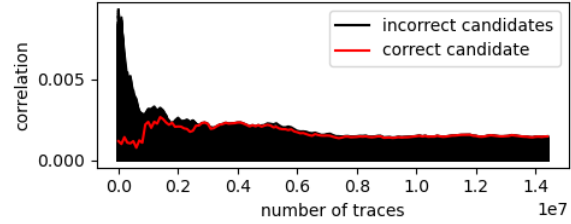


(b) Correlation vs number of traces of the bias in the first layer with the ReLU intermediate.

Figure 10: Key ranks and correlations of the bias with value of 0.856 in the first layer with ReLU intermediate.



(a) Key rank vs number of traces of the bias in the second layer with the  $W * M + b$  intermediate.



(b) Correlation vs number of traces of the bias in the second layer with the  $W * M + b$  intermediate.

Figure 11: Key ranks and correlations of the bias with value of 0.345 in the second layer with  $W * M + b$  intermediate.

take more time to recover all the weights, as our attack targets the partial sums in the convolution where we recover the weights one-by-one. In other words, the time it takes to recover all the weights in a kernel scales linearly with the kernel size.

**Batch size.** In our experiments, the batch size is set to 1. However, a larger batch size might not impact the CEMA attack because the same operations could be carried out in parallel with different inputs. This means that two or more intermediate values are calculated at the same time that depend on the same weight or bias. Therefore, the CEMA attack would be applied using the combination of multiple intermediate values.

**Concurrent applications.** The GPU is able to handle and schedule concurrently CUDA functions from multiple applications. This could likely introduce noise in the attacks. However, this highly depends on the required resources for each CUDA function. If a CUDA function takes up most of the GPU resources (e.g. shared memory, registers, etc.), then a different CUDA function will only be scheduled after all the thread blocks in the previous CUDA function finished execution [3].

## 4.2. Single-precision implementations

The implementations for a convolutional layer with ReLU activation and single-precision calculations are very similar to half-precision implementations analyzed in this work. In fact, the single-precision implementations are named the following:

`maxwell_scudnn_128x_k_relu_t_nn_v1`

where

$$k \in \{32, 64, 128\},$$

$$t \in \{\text{small, medium, large, interior}\}.$$

More importantly, the structures of these implementations are also identical to their half-precision counterparts with the exception of using single-precision instructions instead of half-precision instructions. Consequently, our CEMA attack is also applicable for single-precision implementation. However, targeting 32-bit floats significantly increases the search space even if it is limited to the  $[-5, 5]$  interval.

## 4.3. Mitigation

Traditional ways to contain electromagnetic emanation, such as proper shielding or introducing noise to decrease the Signal-to-Noise ratio, could alleviate the problem [38]. Specifically against parameter extraction, one of the possible countermeasures, which is also mentioned in the CSI-NN paper [13], is shuffling [53] the order of multiplications in the layers, which can make it significantly harder for an adversary to recover the weights. Additionally, masking [18, 42], also mentioned in the CSI-NN paper, would provide a way to break the relationship between the side-channel measurements and the processed data. However, this comes at the price of execution speed, which might not be desired in real-time systems.

#### 4.4. Comparison with related work

To the best of our knowledge, no previous work has been able to extract the parameters of neural networks on GPU using physical side-channel.

Author	Platform	Side channel
<b>BarraCUDA</b> (this work)	<b>GPU</b>	EM
Batina, et al. (2019) [13]	microcontroller	EM
Dubet, et al. (2020) [19]	FPGA	Power
Yoshida, et al. (2020) [57]	FPGA	Power
Regazzoni, et al. (2020) [46]	FPGA	EM
Yli-Märyy, et al. (2021) [55]	FPGA	EM
Li, et al. (2022) [33]	FPGA	Power
Joud, et al. (2022) [26]	microcontroller	EM
Gongye et al. (2023) [22]	FPGA	EM

TABLE 1: Comparison with related work.

Previous works have demonstrated parameter extraction on microcontrollers and FPGAs using power or EM side channel as shown in Table 1, but not on GPUs. In addition, these attacks were performed on neural networks with binary parameters [19, 46, 56], 8-bit parameters [13, 22, 32, 57] or 32-bit parameters [13, 26]. In our work, we demonstrate parameter extraction on 16-bit parameters with discussion on extending it to 32-bit parameters. Additionally, the approach presented in this work is scalable because it does not rely on chosen inputs as in [22]. Chosen inputs are not scalable to large neural networks as crafting chosen inputs becomes harder the deeper the target NN is.

#### 5. Conclusions

In this work, we analyze the NVIDIA Jetson Nano GPU, a commonly chosen platform for real-world neural network implementations, for resilience against side-channel attacks that aim to extract the weights of the target NN. First, we establish where the GPU leaks information about the parameters of the target DNN. Subsequently, we demonstrate the extraction of weights and biases of a CNN consisting of two convolutional layers using CEMA. Overall, the neural network implementations of NVIDIA’s TensorRT framework are vulnerable to parameter extraction using electromagnetic side-channel attack despite the networks running in a highly parallel and noisy environment. It remains an open problem to protect their implementations in security or privacy-sensitive applications.

#### Acknowledgments

This work was supported by an ARC Discovery Early Career Researcher Award DE200101577; an ARC Discovery Project number DP210102670; and the Deutsche Forschungsgemeinschaft (DFG, German Research Foundation) under Germany’s Excellence Strategy - EXC 2092 CASA - 390781972. Additionally, this work received funding in the framework of the NWA Cybersecurity Call with project name PROACT with project number

NWA.1215.18.014, which is (partly) financed by the Netherlands Organisation for Scientific Research (NWO). Moreover, Łukasz Chmielewski was partially supported by Ai-SecTools (VJ02010010) project.

#### References

- [1] “Cuda compute capabilities,” <https://docs.nvidia.com/cuda/cuda-c-programming-guide/index.html#compute-capabilities>, accessed: 2022-09-30.
- [2] “Cuda context,” <https://docs.nvidia.com/cuda/cuda-c-programming-guide/index.html#context>, accessed: 2022-09-30.
- [3] <https://developer.download.nvidia.com/CUDA/training/StreamsAndConcurrencyWebinar.pdf>, accessed: 2022-11-30.
- [4] “cuobjdump,” <https://docs.nvidia.com/cuda/cuda-binary-utilities/#usage>, accessed: 2022-09-30.
- [5] “Cuda programming model,” <https://docs.nvidia.com/cuda/cuda-c-programming-guide/index.html#programming-model>, accessed: 2022-09-30.
- [6] “Cuda half2 data type,” [https://docs.nvidia.com/cuda/cuda-math-api/struct\\_half2.html#struct\\_half2](https://docs.nvidia.com/cuda/cuda-math-api/struct_half2.html#struct_half2), accessed: 2022-09-30.
- [7] <https://www.langer-emv.de/en/product/mfa-active-1mhz-up-to-6-ghz/32/mfa-r-0-2-75-near-field-micro-probe-1-mhz-up-to-1-ghz/854>, accessed: 2022-01-25.
- [8] “Tensorrt model inspection,” [https://docs.nvidia.com/deeplearning/tensorrt/archives/tensorrt-821/api/c\\_api/classnvinfer1\\_1\\_1\\_i\\_engine\\_inspector.html](https://docs.nvidia.com/deeplearning/tensorrt/archives/tensorrt-821/api/c_api/classnvinfer1_1_1_i_engine_inspector.html), accessed: 2022-09-30.
- [9] “Nvidia jetson nano,” <https://developer.nvidia.com/embedded/jetson-nano-developer-kit>, accessed: 2022-09-30.
- [10] “Nvidia tensorrt,” <https://developer.nvidia.com/tensorrt>, accessed: 2022-09-30.
- [11] “Tegra x1 system-on-chip,” <http://international.download.nvidia.com/pdf/tegra/Tegra-X1-whitepaper-v1.0.pdf>, accessed: 2022-09-30.
- [12] M. Abadi, A. Agarwal, P. Barham, E. Brevdo, Z. Chen, C. Citro, G. S. Corrado, A. Davis, J. Dean, M. Devin, S. Ghemawat, I. Goodfellow, A. Harp, G. Irving, M. Isard, Y. Jia, R. Jozefowicz, L. Kaiser, M. Kudlur, J. Levenberg, D. Mané, R. Monga, S. Moore, D. Murray, C. Olah, M. Schuster, J. Shlens, B. Steiner, I. Sutskever, K. Talwar, P. Tucker, V. Vanhoucke, V. Vasudevan, F. Viégas, O. Vinyals, P. Warden, M. Wattenberg, M. Wicke, Y. Yu, and X. Zheng, “TensorFlow: Large-scale machine learning on heterogeneous systems,” 2015, software available from tensorflow.org. [Online]. Available: <https://www.tensorflow.org/>
- [13] L. Batina, S. Bhasin, D. Jap, and S. Picek, “CSI-NN: Reverse engineering of neural network architectures through electromagnetic side channel,” in *28th USENIX Security Symposium USENIX Security 19*, 2019, pp. 515–532.

- [14] E. Brier, C. Clavier, and F. Olivier, “Correlation power analysis with a leakage model,” in *International workshop on cryptographic hardware and embedded systems*. Springer, 2004, pp. 16–29.
- [15] C. Canovas and J. Clédière, “What do s-boxes say in differential side channel attacks?” *Cryptology ePrint Archive*, 2005.
- [16] Ł. Chmielewski and L. Weissbart, “On reverse engineering neural network implementation on GPU,” in *International Conference on Applied Cryptography and Network Security*. Springer, 2021, pp. 96–113.
- [17] F. Chollet, “Xception: Deep learning with depthwise separable convolutions,” in *Proceedings of the IEEE conference on computer vision and pattern recognition*, 2017, pp. 1251–1258.
- [18] J.-S. Coron and L. Goubin, “On boolean and arithmetic masking against differential power analysis,” in *Cryptographic Hardware and Embedded Systems—CHES 2000: Second International Workshop Worcester, MA, USA, August 17–18, 2000 Proceedings 2*. Springer, 2000, pp. 231–237.
- [19] A. Dubey, R. Cammarota, and A. Aysu, “Maskednet: The first hardware inference engine aiming power side-channel protection,” in *IEEE International Symposium on Hardware Oriented Security and Trust*, 2020, pp. 197–208.
- [20] F. Elibol, U. Sarac, and I. Erer, “Realistic eavesdropping attacks on computer displays with low-cost and mobile receiver system,” in *2012 Proceedings of the 20th European Signal Processing Conference (EUSIPCO)*. IEEE, 2012, pp. 1767–1771.
- [21] B. J. Gilbert Goodwill, J. Jaffe, P. Rohatgi *et al.*, “A testing methodology for side-channel resistance validation,” in *NIST non-invasive attack testing workshop*, vol. 7, 2011, pp. 115–136.
- [22] C. Gongye, Y. Luo, X. Xu, and Y. Fei, “Side-channel-assisted reverse-engineering of encrypted dnn hardware accelerator ip and attack surface exploration,” in *IEEE Symposium on Security and Privacy*, 2024.
- [23] K. He, X. Zhang, S. Ren, and J. Sun, “Deep residual learning for image recognition,” in *Proceedings of the IEEE conference on computer vision and pattern recognition*, 2016, pp. 770–778.
- [24] Z. Hongxin, H. Yuewang, W. Jianxin, L. Yinghua, and Z. Jinling, “Recognition of electro-magnetic leakage information from computer radiation with SVM,” *Computers & Security*, vol. 28, no. 1-2, pp. 72–76, 2009.
- [25] A. G. Howard, M. Zhu, B. Chen, D. Kalenichenko, W. Wang, T. Weyand, M. Andreetto, and H. Adam, “Mobilenets: Efficient convolutional neural networks for mobile vision applications,” *arXiv preprint arXiv:1704.04861*, 2017.
- [26] R. Joud, P.-A. Moëllic, S. Pontié, and J.-B. Rigaud, “A practical introduction to side-channel extraction of deep neural network parameters,” in *International Conference on Smart Card Research and Advanced Applications*. Springer, 2022, pp. 45–65.
- [27] P. Kocher, J. Jaffe, and B. Jun, “Differential power analysis,” in *Annual international cryptology conference*. Springer, 1999, pp. 388–397.
- [28] P. C. Kocher, “Timing attacks on implementations of Diffie-Hellman, RSA, DSS, and other systems,” in *Annual International Cryptology Conference*. Springer, 1996, pp. 104–113.
- [29] A. Krizhevsky, I. Sutskever, and G. E. Hinton, “Imagenet classification with deep convolutional neural networks,” *Advances in neural information processing systems*, vol. 25, pp. 1097–1105, 2012.
- [30] M. G. Kuhn and R. J. Anderson, “Soft tempest: Hidden data transmission using electromagnetic emanations,” in *International Workshop on Information Hiding*. Springer, 1998, pp. 124–142.
- [31] N. Laptev, J. Yosinski, L. E. Li, and S. Smly, “Time-series extreme event forecasting with neural networks at uber,” in *International conference on machine learning*, vol. 34. sn, 2017, pp. 1–5.
- [32] G. Li, M. Tiwari, and M. Orshansky, “Power-based attacks on spatial DNN accelerators,” *ACM J. Emerg. Technol. Comput. Syst.*, vol. 18, no. 3, pp. 58:1–58:18, 2022. [Online]. Available: <https://doi.org/10.1145/3491219>
- [33] ———, “Power-based attacks on spatial dnn accelerators,” *ACM Journal on Emerging Technologies in Computing Systems*, vol. 18, no. 3, pp. 1–18, 2022.
- [34] M. Lin, Q. Chen, and S. Yan, “Network in network,” *arXiv preprint arXiv:1312.4400*, 2013.
- [35] L. Liu, W. Ouyang, X. Wang, P. Fieguth, J. Chen, X. Liu, and M. Pietikäinen, “Deep learning for generic object detection: A survey,” *International journal of computer vision*, vol. 128, no. 2, pp. 261–318, 2020.
- [36] Z. Liu, N. Samwel, L. Weissbart, Z. Zhao, D. Lauret, L. Batina, and M. Larson, “Screen gleaning: A screen reading tempest attack on mobile devices exploiting an electromagnetic side channel,” *arXiv preprint arXiv:2011.09877*, 2020.
- [37] H. T. Maia, C. Xiao, D. Li, E. Grinspan, and C. Zheng, “Can one hear the shape of a neural network?: Snooping the GPU via magnetic side channel,” in *31st USENIX Security Symposium, USENIX Security 2022, Boston, MA, USA, August 10-12, 2022*, K. R. B. Butler and K. Thomas, Eds. USENIX Association, 2022, pp. 4383–4400. [Online]. Available: <https://www.usenix.org/conference/usenixsecurity22/presentation/maia>
- [38] S. Mangard, E. Oswald, and T. Popp, *Power analysis attacks: Revealing the secrets of smart cards*. Springer Science & Business Media, 2008, vol. 31.
- [39] A. Moradi, B. Richter, T. Schneider, and F.-X. Standaert, “Leakage detection with the x2-test,” *IACR Transactions on Cryptographic Hardware and Embedded Systems*, pp. 209–237, 2018.
- [40] D. W. Otter, J. R. Medina, and J. K. Kalita, “A survey of the usages of deep learning for natural language processing,” *IEEE transactions on neural networks and learning systems*, vol. 32, no. 2, pp. 604–624, 2020.
- [41] A. Paszke, S. Gross, F. Massa, A. Lerer, J. Bradbury,

G. Chanhan, T. Killeen, Z. Lin, N. Gimelshein, L. Antiga, A. Desmaison, A. Kopf, E. Yang, Z. DeVito, M. Raison, A. Tejani, S. Chilamkurthy, B. Steiner, L. Fang, J. Bai, and S. Chintala, “Pytorch: An imperative style, high-performance deep learning library,” in *Advances in Neural Information Processing Systems 32*. Curran Associates, Inc., 2019, pp. 8024–8035. [Online]. Available: <http://papers.neurips.cc/paper/9015-pytorch-an-imperative-style-high-performance-deep-learning-library.pdf>

[42] E. Prouff and M. Rivain, “Masking against side-channel attacks: A formal security proof,” in *Advances in Cryptology–EUROCRYPT 2013: 32nd Annual International Conference on the Theory and Applications of Cryptographic Techniques, Athens, Greece, May 26–30, 2013. Proceedings 32*. Springer, 2013, pp. 142–159.

[43] H. Purwins, B. Li, T. Virtanen, J. Schlüter, S.-Y. Chang, and T. Sainath, “Deep learning for audio signal processing,” *IEEE Journal of Selected Topics in Signal Processing*, vol. 13, no. 2, pp. 206–219, 2019.

[44] J.-J. Quisquater and D. Samyde, “ElectroMagnetic Analysis (EMA): Measures and Counter-Measures for Smart Cards,” in *Smart Card Programming and Security (E-smart 2001)*, ser. Lecture Notes in Computer Science, I. Attali and T. P. Jensen, Eds., vol. 2140. Springer-Verlag, 2001, pp. 200–210.

[45] S. S. Rangapuram, M. W. Seeger, J. Gasthaus, L. Stella, Y. Wang, and T. Januschowski, “Deep state space models for time series forecasting,” *Advances in neural information processing systems*, vol. 31, 2018.

[46] F. Regazzoni, S. Bhasin, A. A. Pour, I. Alshaer, F. Aydin, A. Aysu, V. Beroulli, G. Di Natale, P. Franzon, D. Hely *et al.*, “Machine learning and hardware security: Challenges and opportunities,” in *International Conference on Computer-Aided Design*, 2020, pp. 1–6.

[47] A. Sagheer and M. Kotb, “Time series forecasting of petroleum production using deep lstm recurrent networks,” *Neurocomputing*, vol. 323, pp. 203–213, 2019.

[48] D. Salinas, V. Flunkert, J. Gasthaus, and T. Januschowski, “Deepar: Probabilistic forecasting with autoregressive recurrent networks,” *International Journal of Forecasting*, vol. 36, no. 3, pp. 1181–1191, 2020.

[49] T. Schneider and A. Moradi, “Leakage assessment methodology,” in *International Workshop on Cryptographic Hardware and Embedded Systems*. Springer, 2015, pp. 495–513.

[50] D. Silver, T. Hubert, J. Schrittwieser, I. Antonoglou, M. Lai, A. Guez, M. Lanctot, L. Sifre, D. Kumaran, T. Graepel *et al.*, “Mastering chess and shogi by self-play with a general reinforcement learning algorithm,” *arXiv preprint arXiv:1712.01815*, 2017.

[51] K. Simonyan and A. Zisserman, “Very deep convolutional networks for large-scale image recognition,” *arXiv preprint arXiv:1409.1556*, 2014.

[52] J. G. van Woudenberg, M. F. Witteman, and B. Bakker, “Improving differential power analysis by elastic alignment,” in *Topics in Cryptology–CT-RSA 2011: The Cryptographers’ Track at the RSA Conference 2011, San Francisco, CA, USA, February 14–18, 2011. Proceedings*. Springer, 2011, pp. 104–119.

[53] N. Veyrat-Charvillon, M. Medwed, S. Kerckhof, and F.-X. Standaert, “Shuffling against side-channel attacks: A comprehensive study with cautionary note,” in *Advances in Cryptology–ASIACRYPT 2012: 18th International Conference on the Theory and Application of Cryptology and Information Security, Beijing, China, December 2–6, 2012. Proceedings 18*. Springer, 2012, pp. 740–757.

[54] M. Yan, C. W. Fletcher, and J. Torrellas, “Cache telepathy: Leveraging shared resource attacks to learn DNN architectures,” in *USENIX Security*, 2020, pp. 2003–2020.

[55] V. Yli-Märy, A. Ito, N. Homma, S. Bhasin, and D. Jap, “Extraction of binarized neural network architecture and secret parameters using side-channel information,” in *IEEE International Symposium on Circuits and Systems, ISCAS 2021, Daegu, South Korea, May 22–28, 2021*. IEEE, 2021, pp. 1–5. [Online]. Available: <https://doi.org/10.1109/ISCAS51556.2021.9401626>

[56] V. Yli-Märy, A. Ito, N. Homma, S. Bhasin, and D. Jap, “Extraction of binarized neural network architecture and secret parameters using side-channel information,” in *IEEE International Symposium on Circuits and Systems (ISCAS)*, 2021, pp. 1–5.

[57] K. Yoshida, T. Kubota, S. Okura, M. Shiozaki, and T. Fujino, “Model reverse-engineering attack using correlation power analysis against systolic array based neural network accelerator,” in *IEEE International Symposium on Circuits and Systems (ISCAS)*, 2020, pp. 1–5.